# Experimental Study on Load-carrying Capacity of Orthotropic Steel-Concrete Composite deck under Combined Compression-Bending

Shi, Zhanchong; Veljkovic, Milan; Su, Qingtian

**Publication date**
2022

**Document Version**
Final published version

**Published in**
Proceedings for the 6th fib International Congress 2022

# Experimental Study on Load-carrying Capacity of Orthotropic Steel-Concrete Composite deck under Combined Compression-Bending

Zhanchong Shi[a,b], Milan Veljkovic[b], Qingtian Su[a,c]

[a] *Department of Bridge Engineering, Tongji University, Shanghai 200092, China*

[b] *Department of Engineering Structures, Delft University of Technology, 2628CN Delft，The Netherlands*

[c] *Shanghai Engineering Research Center of High Performance Composite Bridges, Shanghai 200092, China*

ABSTRACT: In order to investigate load-carrying capacity, ductility and plastic development of orthotropic steel-concrete composite deck used in composite girder cable-stayed bridge, six single-point-loaded simply-supported orthotropic steel-concrete composite decks with varying axial compressive forces and different concrete grades were designed and tested. The test results show that the failure modes of all specimens are similar and exhibit cracks of the lower concrete section combined with crushing of the upper concrete section at midspan. The axial compressive force imposed in this test has a neglected effect on elastic stiffness and vertical load-carrying capacity of tested specimens. While the axial compressive force considerably lowers the ductility and plastic development of the orthotropic steel-concrete composite deck under vertical load. Besides, improving concrete grade from C60 to C80 could not help to enhance elastic stiffness, vertical load-carrying capacity, ductility and plastic development of the composite deck.

## 1 INTRODUCTION

Fatigue crack in traditional orthotropic steel bridge deck system has posed a formidable challenge to bridge engineers all over the world because of ever-increasing heavy traffic volumes and higher wheel loads. The main reasons for fatigue cracks are the following: (1) insufficient stiffness of the steel deck plate; (2) excessive stress amplitudes of both the steel deck plate and the welding seams; and (3) inappropriate details, which may result in stress concentration, if they are not handled in a proper way (Shao et al. 2013). Relevant research results (Wolchuk 2006; Mizuguchi et al. 2004; Chen et al. 2012) show that increasing the local stiffness of bridge deck and reducing the number of welds are the fundamental ways to restrain the initiation and propagation of fatigue cracks.

One way to improve the local stiffness of bridge deck is to replace asphalt pavement with concrete structure layer which is connected to steel deck to form steel-concrete composite deck using shear connectors. Battista et al.(2008) and Boeters et al.(2007) proposed reinforced concrete with thickness of 100~150mm to replace asphalt pavement，and this strategy has been applied in rehabilitation of Rio-Niteroi bridge. Zhan et al.(2006) conducted static test on simply-supported flat steel plate-concrete composite deck to investigate its working performance. Test results showed the structural deformation of the deck slab under service load was little, the slab had fairly great rigidity, the reduction of the structural rigidity of the slab under fatigue load was also little and there was still rather great load bearing capacity and safety margin at the state the slab structure failed. Su et al (2016; 2018). explored the load-bearing capacity and concrete crack pattern of orthotropic composite bridge deck with U-shaped ribs.

All these previous studies merely focused on the static or cyclic performance of steel-concrete composite deck only under vertical load. However, the steel-concrete composite deck used in composite girder cable-stayed bridge also sustains large axial compressive force. In this study, six simply-supported orthotropic steel-concrete composite decks under combined compression-bending with varying axial compressive forces and different concrete grades were designed and tested to investigate its vertical load-carrying capacity, ductility and plastic development.

## 2 EXPERIMENTAL PROGRAM

### 2.1 *Specimen design*

The test program included six specimens which were numbered as SN-1, SN-2, SN-3, SN-4, SN-5 and SN-6. All specimens consisted of two parts: the orthotropic steel deck (OSD) with two U-shaped ribs and concrete slab. The orthotropic steel deck was composed of flat steel plate with thickness of 6mm and width of 1440mm and two U-shaped ribs with thickness of 6mm and height of 194mm. The thickness, width and length of concrete slab were 100mm, 1440mm and 4500mm respectively, and concrete slab was strengthened by longitudinal reinforcements with diameter of 20mm and transversal reinforcement with diameter of 12mm spaced at 150mm both in longitudinal and transversal directions. The orthotropic

steel deck and concrete slab were connected to form the steel-concrete composite deck by using headed studs which were spaced at 200mm × 240mm (longitudinal × transversal). And the headed stud was 80mm high with shank diameter of 13mm and head diameter of 22mm.

These specimens were identical aside from the concrete grade and the magnitude of axial compressive force. Therefore, C60 and C80 concrete were employed in SN1 to SN3 and SN4 to SN6, respectively. The axial compressive force varied from 0kN to 3000kN by step of 1500kN, the reason why we chose these grades was that the compressive stress of concrete deck for composite girder cable-stayed bridge varied from 0 to 26MPa, when the designed steel-concrete composite deck was applied at 3000kN axial compressive force, the compressive stress of concrete slab was almost 13 MPa. Details of test specimens are shown in Table 1 and Figure 1.

Table 1. Details of test specimens.

| Number | Height | Width | Length | Concrete grade | Axial compressive force |
|---|---|---|---|---|---|
| | mm | mm | mm | | kN |
| SN-1 | 300 | 1440 | 4500 | C60 | 0 |
| SN-2 | 300 | 1440 | 4500 | C60 | 1500 |
| SN-3 | 300 | 1440 | 4500 | C60 | 3000 |
| SN-4 | 300 | 1440 | 4500 | C80 | 0 |
| SN-5 | 300 | 1440 | 4500 | C80 | 1500 |
| SN-6 | 300 | 1440 | 4500 | C80 | 3000 |

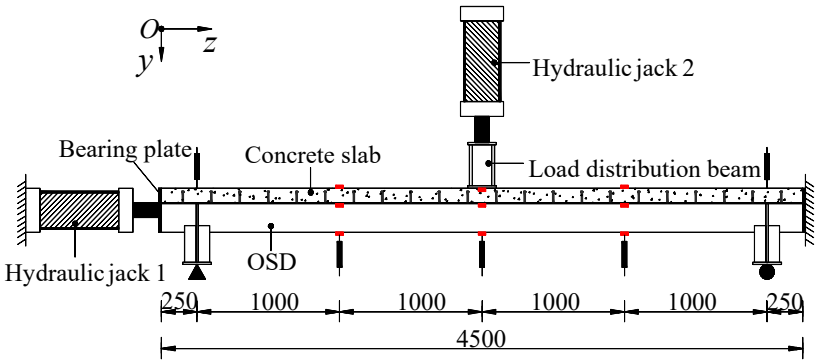


a. Elevation

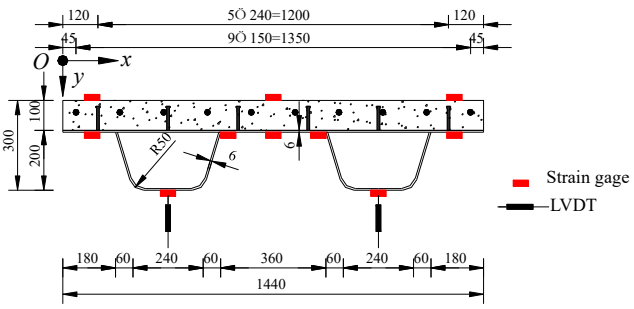


b. Cross-section at midspan

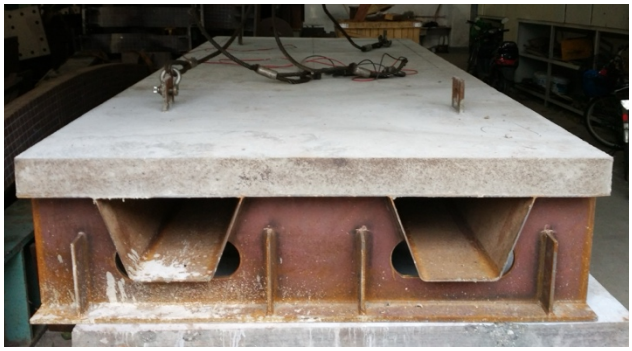

c. Fabricated specimen

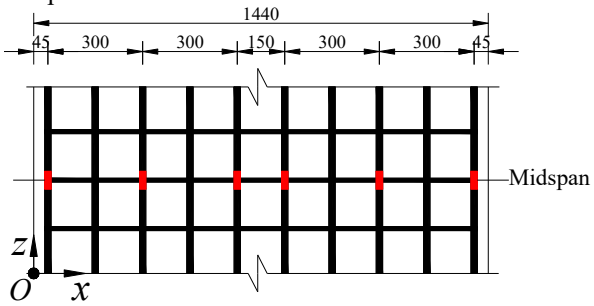


d. Strain gage arrangement of longitudinal reinforcement at midspan

Figure 1. Geometries and instrumentation of the tested specimens (unit: mm).

## 2.2 *Material properties*

The orthotropic steel deck was made of Chinese Q345, two types of thickness of 6mm for flat steel plate and U-shaped ribs and of 16mm for diaphragm were used. HRB400 was utilized for longitudinal and transversal reinforcements. The elastic modulus, yield strength and ultimate strength of steel structure measured according to the Chinese Standard GB/T 228.1-2010 are listed in Table2. The concrete slab used two concrete grades:C60 and C80, and compressive strength and splitting tensile

strength of 150mm concrete cube and elastic modulus of concrete prism with dimension of 100 × 100 × 300mm obtained on the test day are summarized in Table3.

Table 2. Material properties of steel structures.

| Material | $t$ | $d$ | | $f_y$ | $f_u$ |
|---|---|---|---|---|---|
| | mm | mm | MPa | MPa | MPa |
| Structural steel | 6 | - | $2.06\times10^5$ | 378 | 544 |
| | 16 | - | $2.06\times10^5$ | 356 | 540 |
| Reinforcement | - | 12 | $2.00\times10^5$ | 434 | 559 |
| | - | 20 | $2.00\times10^5$ | 477 | 625 |

Note: $E_s$=modulus of elasticity; $f_y$=yield strength; $f_u$=ultimate strength.

Table 3. Material properties of concrete.

| Grade | $E_c$ | $f_c$ | $f_{ct}$ |
|---|---|---|---|
| | MPa | MPa | MPa |
| C60 | 42699 | 64 | 4.5 |
| C80 | 46484 | 81 | 4.2 |

Note: $E_c$=modulus of elasticity; $f_c$= compressive strength; $f_{ct}$= splitting tensile strength.

### 2.3 *Test setup and instrumentation*

Figure 2. Test setup in the field

Figure 2. illustrates the loading test setup in the field. The steel-concrete composite deck was simply supported and subjected to both axial compressive force imposed by horizontal hydraulic jack 1 and vertical force applied through vertical hydraulic jack 2. Therefore, every composite section along the composite deck longitudinal direction sustained axial compressive force, bending moment and shear force. In order to enable the steel-concrete composite deck to be loaded uniformly, a loading distribution beam was attached to the concrete surface along the width direction at midspan. Besides, two bearing steel plates were welded to the two ends of specimen respectively to ease the enforcement of axial compressive force.

The loading protocol included two phases: enforcement of axial compressive force and the enforcement of vertical force. First, horizontal hydraulic jack 1 imposed load to the target value（1500kN or 3000kN）and was kept at this level until the final failure of the specimen. After the axial compressive force reaching its target value, the vertical force was applied to almost 70% of the ultimate vertical force (which was calculated according to theory analysis and numerical simulation) through step-wise load application. Then, the step-wise loading was changed to displacement control based on the midspan vertical displacement of the specimen until the final failure.

The structural response during loading was captured through use of visual observations and electronic instrumentations. The electronic instrumentations included nine electronic resistance strain gages mounted on the concrete, 21 electronic resistance strain gages mounted on the OSD, 18 electronic resistance strain gages mounted on the longitudinal reinforcement, eight LVDTs monitoring vertical deflections of midspan, 1/4 span and bearing points. The locations for strain gages, LVDTs and measuring points arrangement of midspan section are depicted in Figure 1.

## 3 EXPERIMENTAL RESULTS AND ANALYSIS

### 3.1 *Axial load response*

The objective of this research program is to evaluate the structural performance of steel-concrete composite deck used in steel-concrete composite girder cable-stayed bridge of which the deck system is under both axial compressive force and bending moment. Specimens SN-2 and SN-5 sustained axial compressive force of 1500kN, SN-3 and SN-6 were subjected to axial compressive force of 3000kN. The strain distributions along the composite section at midspan of tested specimens only under axial load are depicted in Figure 3.

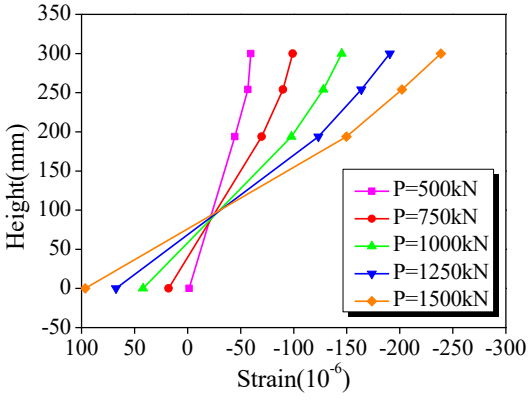


a. SN-2

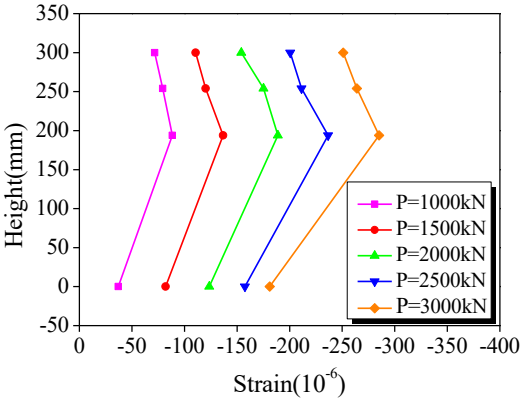


b. SN-3

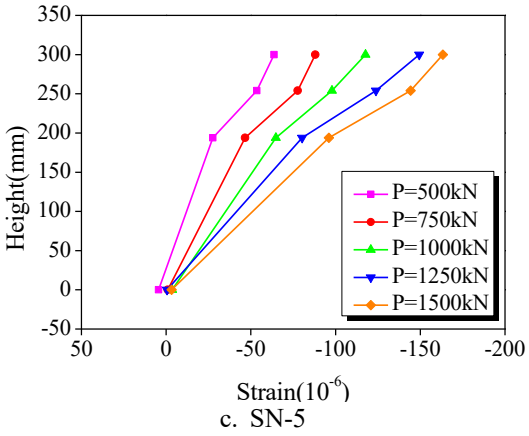


c. SN-5

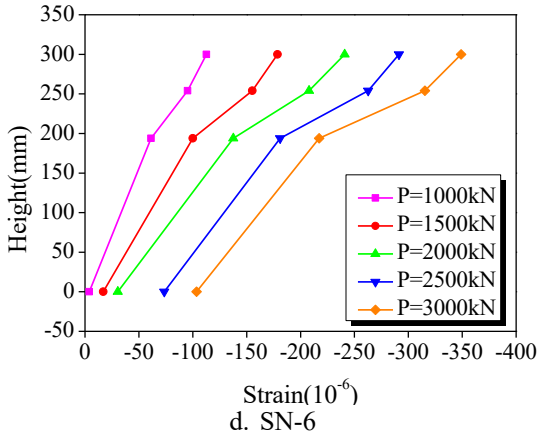


d. SN-6

Figure 3. Strain distributions at midspan section under axial load

As observed in Figure 3., except for specimen SN-3, the strain distributions along the composite section at midspan exhibit non-uniformity which shows a descending trend from top fiber to bottom fiber. Besides, the strain difference between top and bottom fibers enlarges with the increasing of axial load. Notably, the area within 80mm from bottom fiber of section for specimen SN-2 shows tensile strain. All these phenomena could be interpreted by: first, the horizontal hydraulic jack didn't aim at the centroid of composite section at the beginning and induced initial eccentricity which resulted in the tension of the lower section; second, as the out-of plane stiffness of lower section is smaller than the upper section, the out-of plane bending of composite section toward the lower section led by axial load aggravates the strain difference between top and bottom fibers. It should be noted that the axial load response has a slight effect on the vertical load response, as the strain induced by axial compressive load is significantly smaller than that induced by vertical load which will be explained later.

## 3.2 *Combined axial load-vertical load response*

### 3.2.1 *Test observations and main results*

In general, all specimens behaved similarly after the application of vertical load. The vertical load-deflection response at midspan can be summarized in Figure 4. As depicted in Figure 4., the idealized response can be broken down into four distinct phases which are described below.

Phase I, the elastic phase refers to the global elastic straining of the material before the yielding of bottom flange of U-shaped ribs. It is characterized by an initial linearly elastic response. With the increasing of vertical load, the strain at bottom flange of U-shaped ribs reaches yield strain at the load of Py. Py refers to the yielding load which is close to 50%~60% of the ultimate load Pm, and the deflection corresponding to Py is named as yielding deflection, δy. It should be noted that there is a bang sound when loaded to 20%~50% of Pm at phase I , this is an indication of disappearance of natural adhesion between OSD and concrete slab. Phase II, the initial inelastic phase refers to the developing process of first concrete crack. After passing the yielding point (Py, δy), the neutral axis moves upward and more and more concrete section are becoming to sustain tensile force. The vertical load-deflection response behaves initial inelastic characteristic. At the end of this phase, first transversal concrete crack which could be captured through eyesight appears under crack load Pc which is almost 78%~85% of the ultimate load Pm, and corresponds to crack deflection δy. Phase III, the classic nonlinear phase refers to stage before the failing of specimen. As the vertical load increased above Pc，the global response changed with significantly increased increment of deflection being observed. The specimen initiates failure with crushing of the upper concrete at midspan when loaded to the ultimate load Pm corresponding to summit deflection δy. Phase IV, the collapse phase refers to stage that the deflection continues to develop while the vertical begins to decrease. At the terminal of phase IV, the globe achieves the ultimate deflection δu corresponding to the characteristic load Pu which is approximately 81%~91% of the ultimate load Pm. Accordingly, the specimen is considered to be finally failed at point (Pu, δu). Then the specimen couldn't bear any external force.

The final failure modes of midspan section and shear-bending deformation of stud after moving concrete slab are presented in Fig.5, and the main test results of all specimens are listed in Table 4.

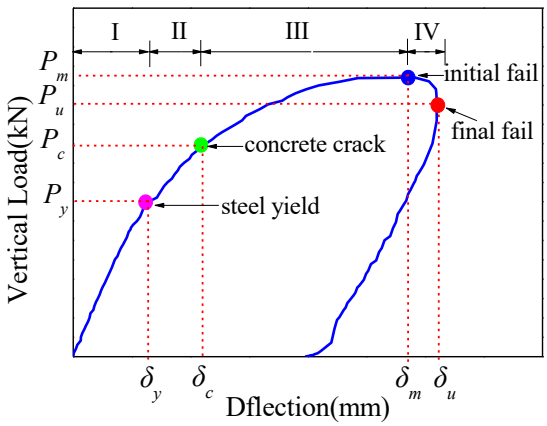


Figure 4. Vertical load-deflection response

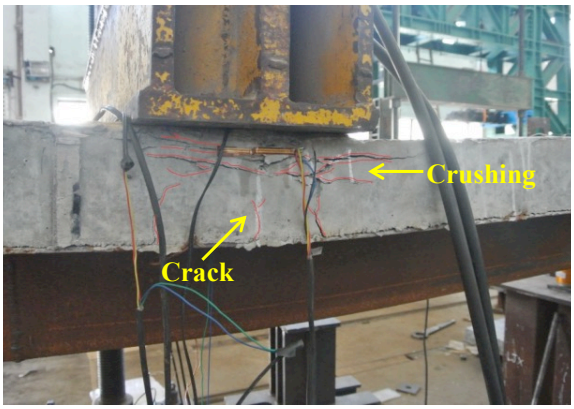


a. Concrete slab


b. Headed stud

Figure 5. Failure modes at midspan section

Table 4. Summary of test results.

| Specimens | $P_y$ | $P_c$ | $P_m$ | $P_u$ | $\delta_y$ | $\delta_c$ | $\delta_m$ | $\delta_u$ | $\mu$ |
|---|---|---|---|---|---|---|---|---|---|
| | kN | kN | kN | kN | mm | mm | mm | mm | |
| SN-1 | 393 | 607 | 726 | 657 | 13.82 | 28.72 | 57.01 | 61.97 | 4.48 |
| SN-2 | 371 | 547 | 718 | 584 | 17.36 | 26.12 | 42.85 | 45.88 | 2.64 |
| SN-3 | 452 | 640 | 755 | 616 | 15.00 | 26.72 | 37.86 | 46.15 | 3.08 |
| SN-4 | 398 | 625 | 789 | 719 | 11.24 | 24.69 | 54.77 | 57.98 | 5.16 |
| SN-5 | 549 | 634 | 765 | 640 | 17.65 | 23.36 | 45.11 | 46.98 | 2.66 |
| SN-6 | 466 | 607 | 775 | 550 | 13.97 | 20.68 | 43.24 | 45.07 | 3.23 |

Note: $P_y$-yielding vertical load, $P_c$-crack vertical load, $P_m$-ultimate vertical load, $P_u$ -charecteristic load; $\delta_y$-yielding deflection, $\delta_c$-crack deflection, $\delta_m$-summit deflection, $\delta_u$-ultimate deflection; $\mu=\delta_u/\delta_y$.

### 3.2.2 *Vertical load-deflection response*

Figure 6. plots the comparison of vertical load-deflection response at midspan of all tested specimens. As can be seen in Fig.6a, both elastic stiffness and the ultimate vertical load of specimen SN-1、SN-2 and SN-3 are almost equal to each other. It indicates that the influence of axial compressive force of 1500kN and 3000kN on initial stiffness and load-carrying capacity of the steel-concrete composite deck could be neglected. This is because the initial axial compressive force is small compared to the ultimate vertical load. The phenomenon and causes also pertain to the comparisons among specimen SN-4、SN-5 and SN-6 which are plotted in Figure 6b.

However, compared with specimens sustained axial compressive force, specimens without axial compressive force experiences a significantly longer developing process from steel yielding to global failure. This also can be captured by ductility coefficient μ(Guo et al. 2018)(see Table 4)，which is defined as the ratio of δu to δy and refers to the ability of a structure or member to maintain inelastic deformation and to dissipate elastic potential energy before failure with constant load-carrying capacity. The ductility coefficient μ of specimens without axial compressive force are almost 1.5~1.9 times to that subjected to axial compressive force. Therefore, it could be concluded that the axial compressive force has a negative effect on the ductility of the steel-concrete composite deck under vertical load.

As presented in Fig.6c~Fig.6e and Table 4, the elastic stiffness and ductility coefficient μ of specimens which sustain axial compressive force or not enhance slightly when improving concrete grade from C60 to C80. Moreover, the vertical load-carrying capacity of specimens has been enhanced at varying degrees, and corresponding increase ratios are 9%, 7% and 3% for specimen SN1 to SN4, SN2 to SN5 and SN3 to SN6. This could be interpreted by the fact that the elastic stiffness is determined from section size and modulus of elasticity，so improving C60 to C80 does not have significant effect on elastic stiffness. Besides, concrete area bearing compression is very small with the moving up of the neutral axis at the terminal of Phase III(discussed above),so the compressive strength does not play a major role in ultimate load. Therefore, improving concrete grade could not help to enhance vertical load-carrying capacity considerably. Obviously, it also appears that increase ratios of vertical load-carrying capacity exhibits a descending trend with axial compressive force varying from 0kN to 3000kN.

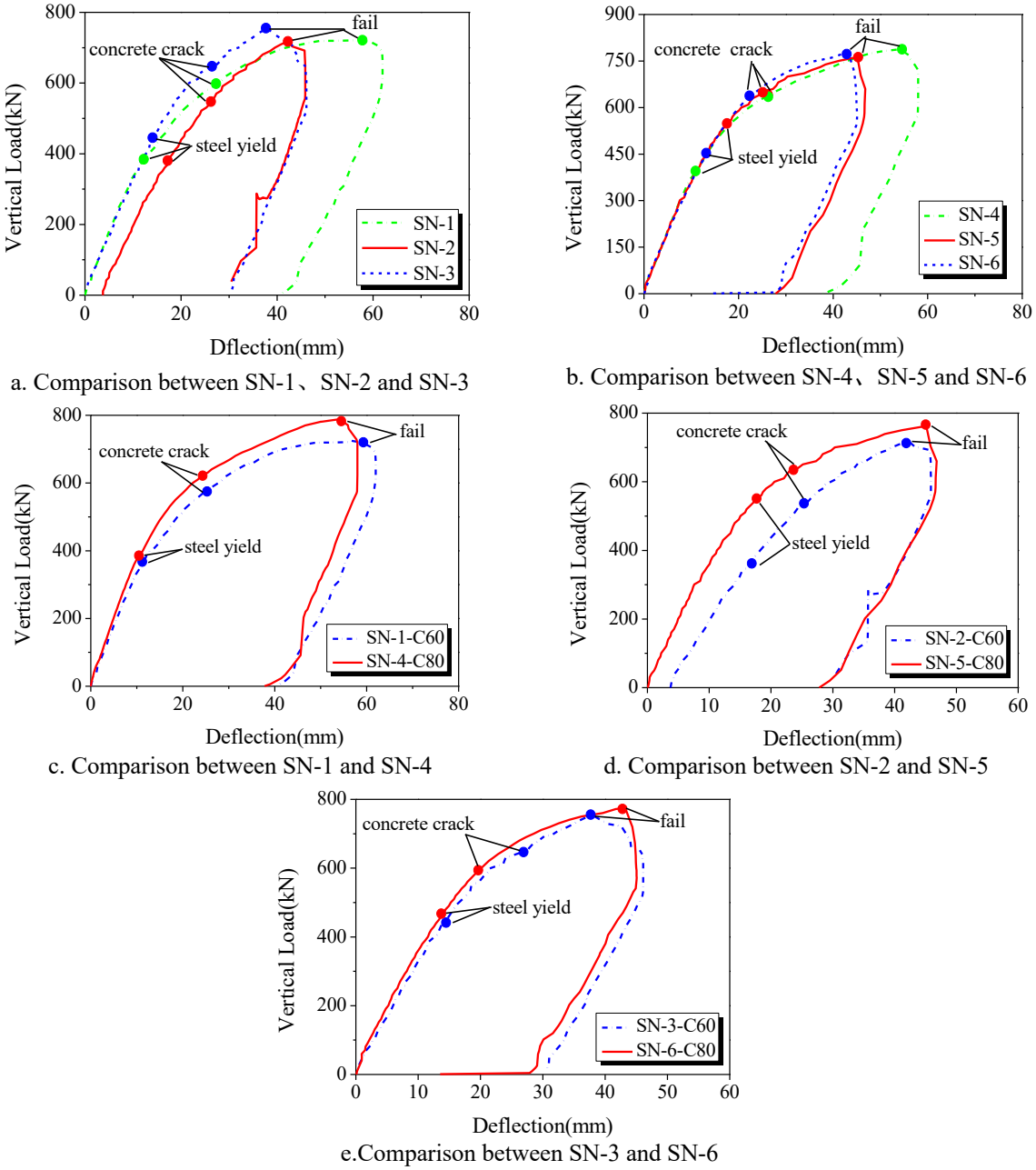


Figure 6. Vertical load-deflection response

### 3.2.3 *Strain distribution*

The strain distributions along height of composite cross section at midspan under varying vertical load are illustrated in Figure 7. And the strain is taken as the mean value of different measuring points of concrete slab, longitudinal reinforcements, flat steel plate and U-shaped ribs in transversal direction. As shown, the strain distribution of all tested specimens remains linear up to about 80% of the ultimate vertical load no matter the specimen is subjected to axial compressive force. This demonstrates two conclusions, one is the arrangement of headed studs achieves perfect composite effect between OSD and concrete slab which contributes to the plane-section assumption of composite section, so it could be applied in steel and concrete composite deck. The other one is the strain induced by axial compressive force is too small to consider compare to that led by vertical load.

Taking the midspan sections of specimens SN1 and SN-4 as examples, Figure 8. presents the developing process of location of the neutral axis under different levels of vertical load. As shown, the location of the neutral axis moves toward concrete slab with increased vertical load, and more and more concrete area is becoming to sustain tension.

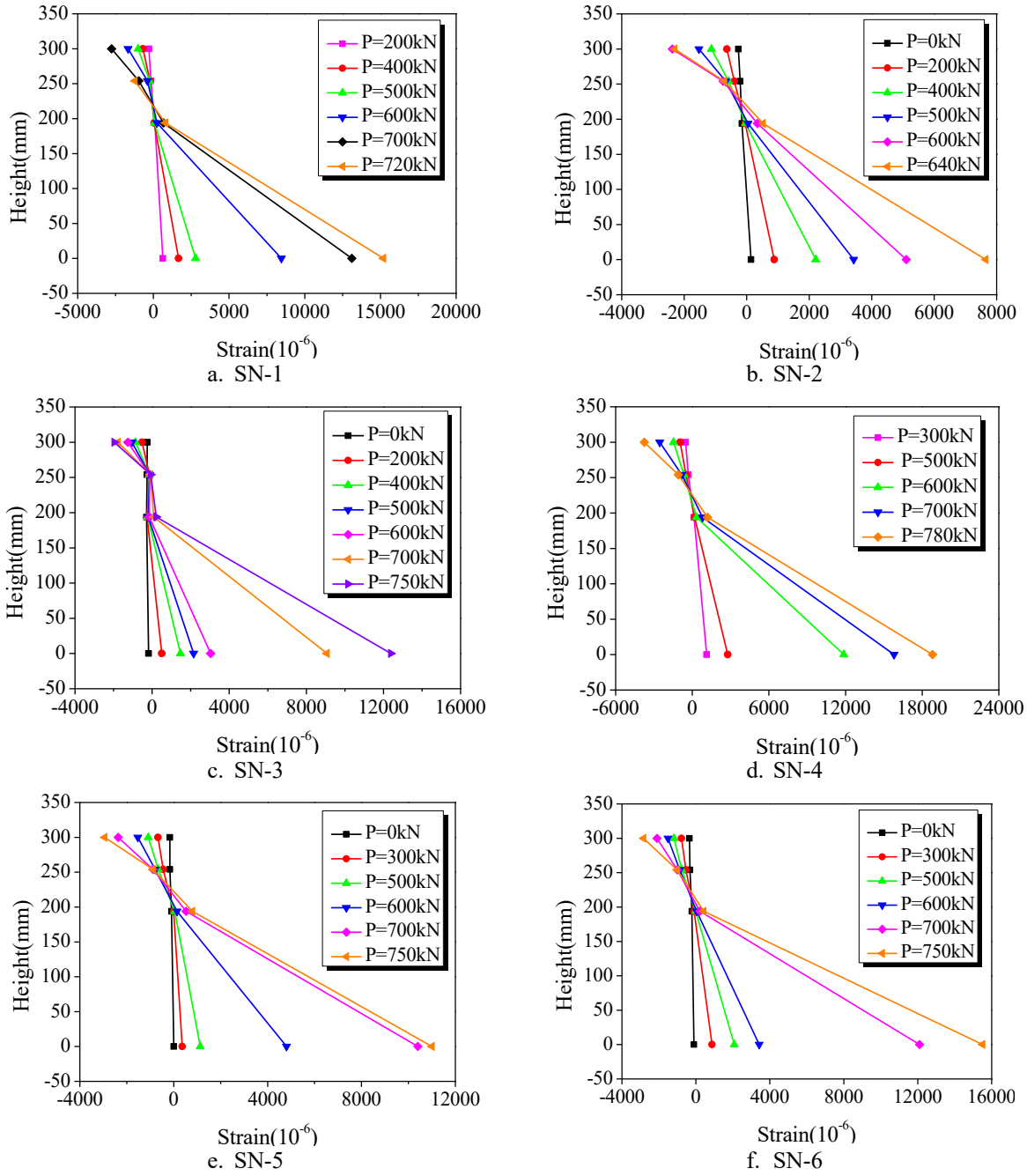


Figure 7. Strain distribution along height of section at midspan.

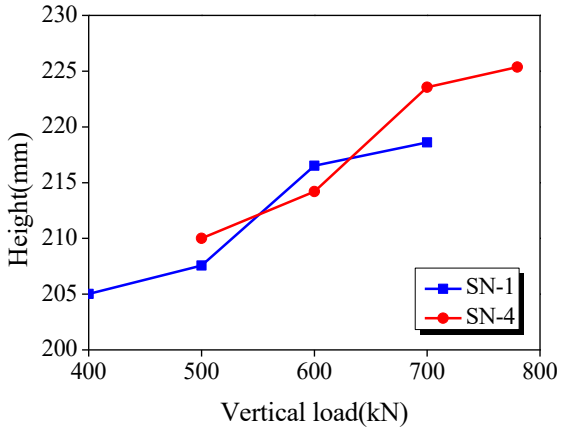


Figure 8. Neutral axis locations under different loading levels

### 3.2.4 *Plastic development analysis*

Neglecting the limited plasticity propogated in elastic phase, namely phase I, the plastic development process of steel-concrete composite decks could be considered from yielding (point(Py, δy))of OSD to final crushing(point(Pu, δu)). Therefore, deflection increment δu-δy at midspan could denote the plastic development of the

globe. Fig.9 summarizes deflection increment of plastic development for all tested specimens. As shown, deflection increments δu-δy of specimen both SN-1 and SN-4 surpasses 45mm, while that of specimens sustained axial compressive force are just around 30mm. It indicates that axial compressive force is negative to the plastic development of steel-concrete composite deck under vertical load. Moreover, plastic development of steel-concrete composite deck has not been improved when improving concrete grade from C60 to C80, with the comparisons between SN-1 and SN-4, SN-2 and SN-5, SN-3 and SN-6 respectively.

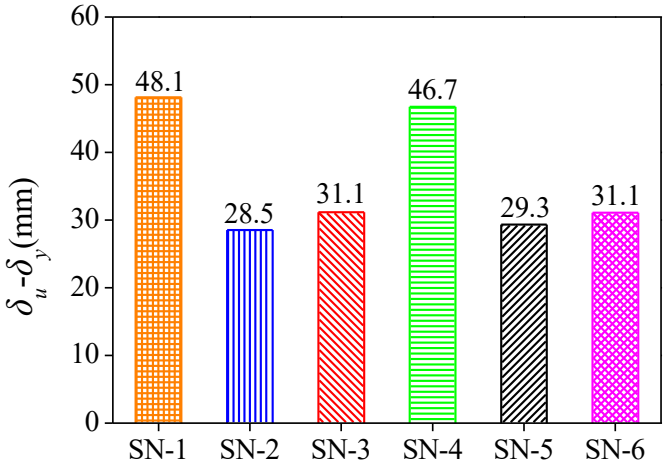

Figure 9. Deflection increment of plastic development.

## 4 CONCLUSION

In this study, six single-point-loaded simply-supported orthotropic steel-concrete composite decks with varying axial compressive forces and different concrete grades were designed and tested to evaluate the load-carrying capacity of composite deck. The main conclusions can be drawn as follows:

1) The final failure modes of all specimens are characterised by cracks in the lower concrete section and crushing of the upper concrete section at midspan.

2) The axial compressive force of 1500kN and 3000kN has a neglected effect on the elastic stiffness and vertical load-carrying capacity of tested specimens. While the axial compressive force considerably lower the ductility of the steel-concrete composite deck under vertical load.

3) The elastic stiffness, vertical load-carrying capacity and ductility of steel-concrete composite deck could not be significantly enhanced when improving concrete grade from C60 to C80.

4）When changing concrete from C60 to C80, increase ratios of vertical load-carrying capacity exhibits a descending trend with axial compressive force varying from 0kN to 3000kN.

5) The strain distribution along height of composite section conforms to plane-section assumption, which demonstrates that the arrangement of headed studs achieves perfect composite effect between OSD and concrete slab. And the strain induced by axial compressive force is too small to consider compared to that led by vertical load.

6) Axial compressive force is negative to the plastic development of steel-concrete composite deck under vertical load. Besides, improving concrete grade from C60 to C80 could not help to enhance the plastic development of steel-concrete composite deck.

## REFERENCE


[1] Shao, X.D. et al. (2013). Basic performance of the composite deck system composed of orthotropic steel deck and ultrathin RPC layer. *J.Bridge Eng. 18 (5)*, 417-428.

[2] Wolchuk, R. (2006). Prefabricating standard orthotropic steel decks. *Modern Steel Construction 12*, 49-51.

[3] Mizuguchi, K et al. (2004). Rationalized steel deck structure and large model test for developing new type of structure. *Orthotropic Bridge Conference,Sacramento*, 675-688.

[4] Chen, H.T. et al. (2012).Comparative analysis of fatigue stress in longitudinal rib and cover plate joints of orthotropic steel deck plate. *Bridge Construction 42 (6)*, 20-26.

[5] Battista, R C et al. 2008. Fatigue life estimates for a slender orthotropic steel deck. *Journal of Constructional Steel Research 64(1)*,134-143.

[6] Boeters, A G. 2007. Concrete overlay of movable steel orthotropic bridges: The repair method for movable steel bridges. M.S. thesis, Delft University of Technology.

[7] Zhan, Y.L., Zhao R.D., Mao X.M., & Mou T.M. (2006). Experiment of mechanical behavior of steel and concrete composite deck slab under positive bending moment. *Bridge Construction (05)*,5-8.

[8] Su, Q.T. et al. (2016). Performance of the orthotropic composite bridge dec k with U-shape stiffener. *Journal of Harbin Institute of Technology 48(09)*:14-19.

[9] Su, Q.T., Dai C.Y., & Xu C.. (2018). Full-scale experimental study on the negative flexural behavior of orthotropic steel-concrete composite bridge deck. *J.Bridge Eng. 23 (12)*: 04018097.

[10] General Administration of Quality Supervision, Inspection and Quarantine of the People's Republic of China and the Standardization Administration of the People's Republic of China. (2010). Metallic materials—Tensile testing—Part 1: Method of test at room temperature GB/T 228.1-2010. Beijing, *China Communications Press*.

[11] Guo, L.H., Liu Y., & Qu B.. (2018). Fully composite beams with U-shaped steel girders: Full-scale tests, computer simulations, and simplified analysis models. *Engineering Structures 177*:724-738.